Mechanochemical actuators of embryonic epithelial contractility

YongTae Kim[a,1], Melis Hazar[a], Deepthi S. Vijayraghavan[b], Jiho Song[a], Timothy R. Jackson[b], Sagar D. Joshi[b,2], William C. Messner[c,3,4], Lance A. Davidson[d,4], and Philip R. LeDuc[e,4]

[a]Department of Mechanical Engineering, Carnegie Mellon University, Pittsburgh, PA 15213; [b]Department of Bioengineering, University of Pittsburgh, Pittsburgh, PA 15260; [c]Departments of Mechanical Engineering and Electrical and Computer Engineering and Robotics Institute, Carnegie Mellon University, Pittsburgh, PA 15213; [d]Departments of Bioengineering, Developmental Biology, and Computational and Systems Biology, University of Pittsburgh, Pittsburgh, PA 15260; and [e]Departments of Mechanical Engineering, Biomedical Engineering, Computational Biology, and Biological Sciences, Carnegie Mellon University, Pittsburgh, PA 15213

Edited by Shu Chien, University of California, San Diego, La Jolla, CA, and approved August 18, 2014 (received for review March 20, 2014)

Spatiotemporal regulation of cell contractility coordinates cell shape change to construct tissue architecture and ultimately directs the morphology and function of the organism. Here we show that contractility responses to spatially and temporally controlled chemical stimuli depend much more strongly on intercellular mechanical connections than on biochemical cues in both stimulated tissues and adjacent cells. We investigate how the cell contractility is triggered within an embryonic epithelial sheet by local ligand stimulation and coordinates a long-range contraction response. Our custom microfluidic control system allows spatiotemporally controlled stimulation with extracellular ATP, which results in locally distinct contractility followed by mechanical strain pattern formation. The stimulation–response circuit exposed here provides a better understanding of how morphogenetic processes integrate responses to stimulation and how intercellular responses are transmitted across multiple cells. These findings may enable one to create a biological actuator that actively drives morphogenesis.

microfluidics | multicellular | mechanotransduction | signaling

Physiological control systems have evolved diverse strategies to sense the environment, transduce signals, and actuate contractile responses. One such strategy involves the actuation of nonmuscle cell contractility to drive a wide range of developmental processes as well as normal physiological and pathological disease states (1–5). The contractile behaviors of cells and their interactions in multicellular arrays are not only critical in shaping and guiding tissue formation (e.g., epithelial folding) for the successful outcome of development programs (6, 7), but also play a major role in the pathology of tumor growth, the invasion-metastasis cascade, wound healing, and tissue regeneration (8, 9).

From a signaling standpoint, embryonic development is a dynamic process where cells interact and coordinate force generation as their identities are patterned by spatiotemporally applied chemical stimuli. There has been considerable debate over the effectiveness of intra- versus intercellular signaling during development (10, 11); nevertheless, the cell–cell signaling and the coordination of a variety of multicellular responses are known to be mediated by gap-junction-dependent intercellular communication (12, 13). However, recent findings from studies of cell mechanics indicate that mechanical cues can be as potent as chemical factors in directing cell differentiation and behaviors and suggest a role in modulating signal transduction pathways (14, 15). Less clear is whether signal transduction can be modulated by mechanical connections during morphogenesis.

Results and Discussion

To investigate the complex integrated response of a multicellular system and investigate the mechanochemical response and actuation, we cultured an intact epithelial sheet adhered to a fibronectin extracellular matrix substrate within a custom microfluidic chamber and exposed a narrow band of 4–5 cells within the sheet to ATP (Fig. 1 *A* and *B*). ATP can trigger contraction in the *Xenopus* embryonic epithelium to the same degree as cell lysate (16). Extracellular ATP has been shown to activate contraction in a range of cell types from endothelial cells of the cardiovascular system to skeletal muscle cells (17). Cells exposed to a stream of ATP for 10 s contract and subsequently relax over 3 min. Using this stimulation protocol, we identified a level of stimulation (50-μM ATP) that consistently triggered contraction (Fig. S1) and produced distinct patterns of local strain in the tissue (Fig. 1 *C–E*; for details on strain maps see *Materials and Methods*). The threshold level of ATP concentration does not depend on the stimulation duration as long as it is not longer than 20 s, which is a limitation due to the delay between ATP exposure and the contraction response. The contraction response after 20 s causes initially adjacent cells to be drawn into the stream and exposed to ATP, which complicates interpretations of the results due to additional cells being stimulated. We note that the stream delivered to the tissue was strictly laminar with sharp concentration gradients across the stream

Significance

This study shows how cell contractility is triggered within an embryonic epithelial sheet by local ligand stimulation and coordinates a long-range contraction response. The stimulation–response circuit exposed here provides a better understanding of how morphogenetic processes integrate responses to stimulation and how intercellular responses are transmitted across multiple cells. Understanding the systems-level behavior of biological signaling networks may allow us to control biological actuators with engineered spatiotemporal stimulation. Our findings will provide a better understanding of contractility-dependent morphogenetic movements as well as the intercellular communication pathways critical during developmental biology, synthetic morphogenesis, and multicellular mechanotransduction signaling.

Author contributions: Y.K., W.C.M., L.A.D., and P.R.L. designed research; Y.K., M.H., D.S.V., and J.S. performed research; Y.K., M.H., D.S.V., J.S., T.R.J., S.D.J., W.C.M., L.A.D., and P.R.L. contributed new reagents/analytic tools; Y.K., M.H., D.S.V., J.S., T.R.J., W.C.M., L.A.D., and P.R.L. analyzed data; S.D.J. and L.A.D. identified the use of extracellular ATP for inducing contractility in Xenopus embryonic tissues; and Y.K., W.C.M., L.A.D., and P.R.L. wrote the paper.

The authors declare no conflict of interest.

This article is a PNAS Direct Submission.

[1]Present address: The George W. Woodruff School of Mechanical Engineering, Wallace H. Coulter Department of Biomedical Engineering, Institute for Electronics and Nanotechnology, Parker H. Petit Institute for Bioengineering and Bioscience, Georgia Institute of Technology, Atlanta, GA 30332.

[2]Present address: American Air Liquide Inc., Delaware Research and Technology Center, Newark, DE 19702.

[3]Present address: Department of Mechanical Engineering, Tufts University, Medford, MA 02155.

[4]To whom correspondence may be addressed. Email: lad43@pitt.edu, william.messner@tufts.edu, or prl@andrew.cmu.edu.

This article contains supporting information online at www.pnas.org/lookup/suppl/doi:10.1073/pnas.1405209111/-/DCSupplemental.

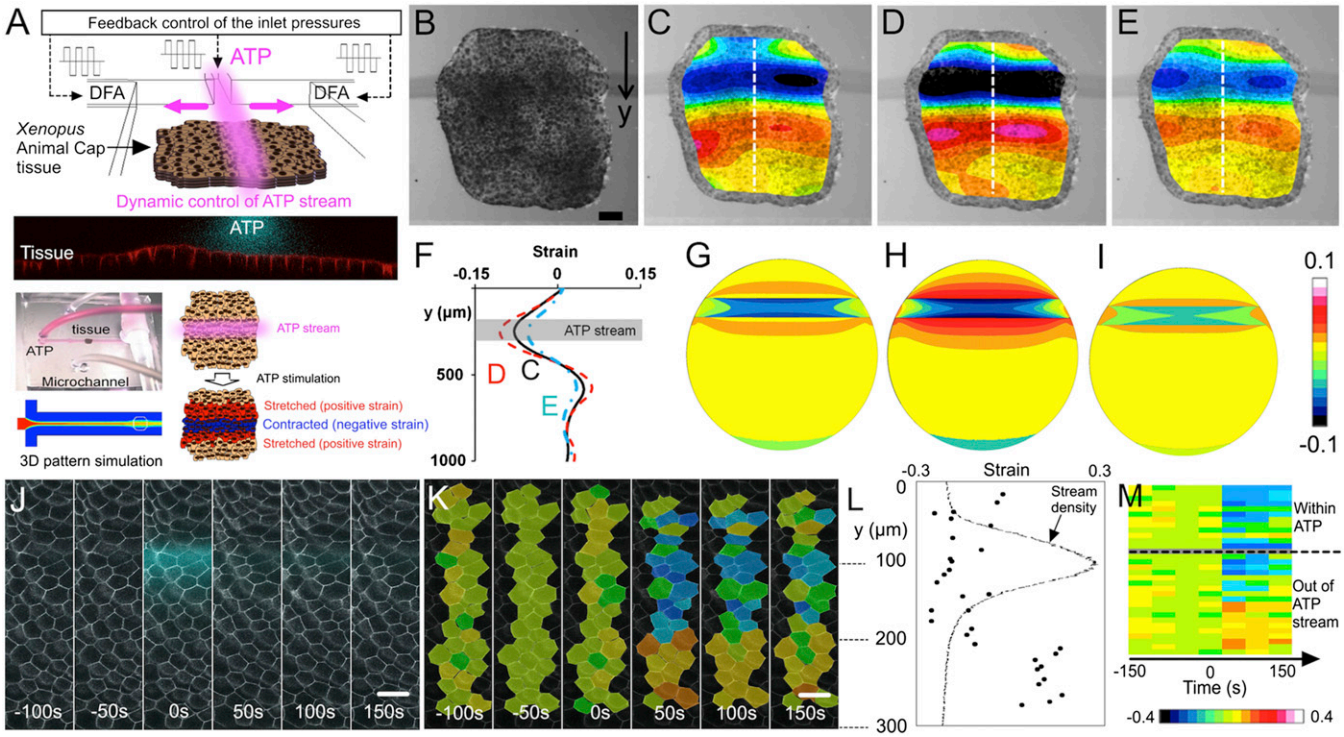

Fig. 1. Understanding mechanochemical actuation through epithelial contractility in an *X. laevis* embryonic tissue. (*A*) Schematic and confocal image (front view) showing microfluidic stream of extracellular ATP applied to a *Xenopus* embryonic tissue. This stream profile was spatiotemporally controlled through our feedback microfluidic control of the inlet pressure at the streams (for the performance of our microfluidic control system see Movie S1) (40–42). Photograph of the microfluidic device, in which a single AC tissue explant is being locally stimulated by the central stream bounded by culture media (DFA). Computation fluid dynamics simulation predicting flow patterns around a tissue model (Movie S2). The cells exposed to a stream of extracellular ATP contract whereas the neighboring cells stretch. (*B*) Microscope image of a *Xenopus* embryonic tissue with a gray stream indicating the location of ATP (for the contractility of the tissue see Movie S3). (Scale bar: 100 μm.) (*C*–*E*) Strain map responses of locally ATP stimulated *Xenopus* tissue indicating mechanical actuation at (*C*) 20-, (*D*) 60-, and (*E*) 100 s after 10-s ATP stimulation. The color maps overlay the corresponding microscope images of the tissue in the microfluidic channel and indicate the strain distribution in the tissue. (*F*) Strains at the middle section of the tissue perpendicular to the stream. The data for the black solid line correspond to the image in *C*, the red dashed line to *D*, and the blue dashed-dotted line to *E*. The gray rectangular area represents the location of the ATP stream that covers the tissue. (*G*–*I*) Strain map responses of locally ATP stimulated tissue modeled with FE analysis. *G*, *H*, and *I* attempt to simulate *C*, *D*, and *E*, respectively. (*J* and *K*) Time-lapse images showing multiple cells of embryonic epithelial sheet in a tissue explant with ATP stream (*J*) and the strains of the cells (*K*) on the tissue (Movie S4). A pulse ATP stream was applied at 0 s and lasted for 45 s. (Scale bar: 50 μm.) Strains were calculated in the direction perpendicular to the stream and normalized to the frame at 50 s before the stream onset (i.e., "−50 s"). (*L*) Maximum strains (dots) of the cells selected in *K* and the ATP stream location and fluorescent intensity (dotted line). (*M*) Strain over time in individual cells organized by proximity to stream. The color coding indicates a gradient in strains where black is the most negative strain and white is the most positive strain. Blocks above the dashed line show the strains of the cells within the ATP stream; blocks below the dashed line are those of the cells out of the stream. The stream position was calculated using 10% of maximum stream intensity criterion (i.e., stream density in *L*).

interfaces (Fig. S2). Because ATP does not diffuse significantly beyond the central stream, this finding suggested that contractile cells beyond the site of direct stimulation received a stimulus from neighboring cells and that the cells in the positive strain regions did not receive a signal and were stretched by the tensile force produced by adjacent contracting cells. We also developed a static structural finite element (FE) model of embryonic tissue to analyze and understand the strain patterns in the tissue (Fig. 1 *G*–*I*). Furthermore, close investigation of the characteristic spatial responses of epithelial contractility at a cellular level demonstrated that stimulation with ATP produced a consistent spatial contraction response more than 6 cell diameters from the site of stimulation and led to subsequent stretching of multiple neighboring cells (Fig. 1 *J*–*M* and Movie S4).

Tissues stimulated with ATP display characteristic temporal responses (Fig. 2 and Movie S5). Tissues pulsed with 5, 10, 20, and 30 s of ATP stimulate neighboring cells at increasing distances (Fig. 2*A* and Fig. S3). The degree and extent of contractile responses were estimated from strain maps (Fig. 2 *B* and *D*), and the domain of cell contraction response expands as the stimulation duration increases (Fig. 2 *C* and *E*). Using the FE model, we mimicked the contractile responses of our experiments (Fig. 2*C*) with strain maps (Fig. 2*F*). Our model produces strain patterns similar to those observed in experiments. Based on previous measurements of the viscoelastic material properties of *Xenopus* embryos (18, 19), the shear modulus ranges from 3 to 15 Pa over these stages. Our FE model shows how tissues displace beyond the area exposed to ATP. The initial contraction responses have a consistent time delay of ∼20 s, whereas the time-to-max is ∼50 s after the onset of the contraction. This timescale for this contraction response is comparable to the timescales reported previously for mechanical or biochemical signal transmission. Whereas a few seconds or milliseconds have been reported in some systems for the timescale of the mechanical and chemical signal transmission (14), this timescale was estimated at a single-cell level and not in a multicellular integrated tissue, which is what our work presents as shown in literature on the timescale for mechanical stimulus transmission of the cycle length of actomyosin fluctuation ranges from 1 to 5 min in the *Drosophila* (20, 21), and *Xenopus* gastrula tissues (22), as well as other induced contractions in *Xenopus* (16). Additionally, we find the signal transmission distance—the distance between the edge of the ATP

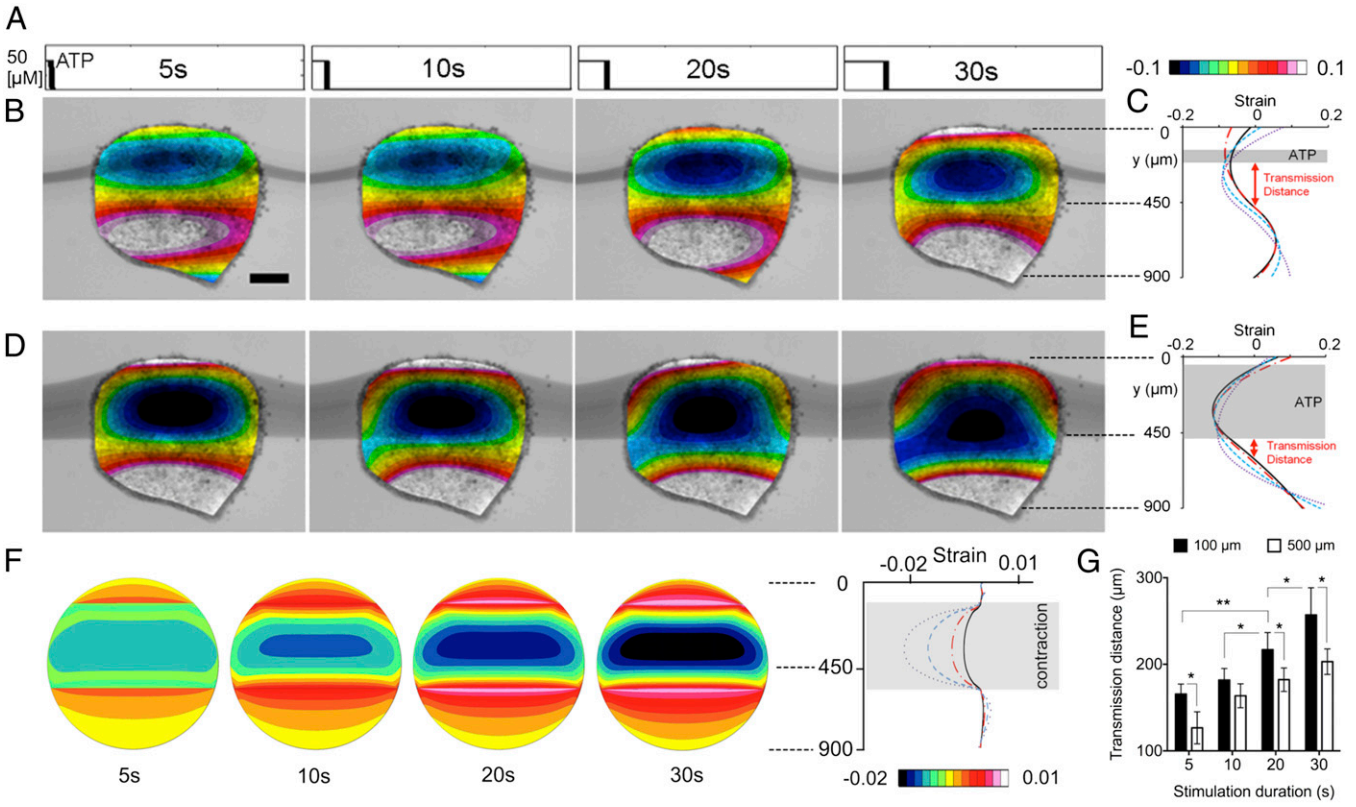

Fig. 2. Contractile actuation response of an embryonic tissue to spatially localized stimulation with pulsed temporal patterns. (*A*) Input stimulation profiles for 5-, 10-, 20-, and 30-s durations of extracellular ATP streams in the microfluidic channel. (*B*–*E*) Strain maps and profiles of a tissue when it was maximally contracted (at 60 s after the stimulation starts) in response to extracellular ATP microfluidic stream (indicated in dark gray) stimulation patterns for two stimulation widths: (*B* and *C*) 100 μm and (*D* and *E*) 500 μm. For each width, the four corresponding images are for the input pulse profiles in *A*. The color map is the strain distribution in the tissue overlaid on the image of tissue. (Scale bar: 200 μm.) Signal transmission distance was defined by the distance between the edge of the ATP stream and the intersection of the negative and positive strains on the strain maps. (*F*) Strain maps from our FE analysis simulate each case in *D*. (*G*) Signal transmission distances for different stream widths: 100 and 500 μm. Error bars represent SDs (* indicates $P < 0.05$, ** indicates $P < 0.01$). $n = 27$ (17 explants).

stream and the intersection of the negative and positive strains on the strain maps—of the contractile response always extends beyond the regions exposed directly to the ATP stream. We observed that the signal was transmitted farther from narrow activating streams than wider streams (Fig. 2*G*). We note that the slope of the graph is not the physical velocity of the spreading contraction, as we need to consider a time delay of 20 s in the mechanism of contractility. We cannot accurately estimate the transmission distance for ATP stimulation durations longer than 20∼30 s because the initial contraction recruits additional cells into the ATP stream.

The contraction response of cells distant from the site of ATP stimulation suggested that intracellular transmission of the stimulation–response signal is mediated (*i*) by traditional secondary messengers via gap junctions, or (*ii*) by mechanically transmitted signals. To identify the roles of these two distinct pathways from these hypotheses, we examined signal transmission after blocking actomyosin contractility or after blocking intracellular gap-junction signaling. We first confirmed that we could inhibit the complete contraction response with blebbistatin (BBS) to inhibit nonmuscle myosin II contractility (23, 24). In most published studies BBS is used to treat the entire field of cells in a dish or all of the tissues in an intact embryo. However, such treatments would obscure any role for actomyosin contractility in mechanotransduction beyond mediating the contractile response. This was the primary motivation for using microfluidics to deliver a narrow stream of BBS that would allow us to test the role of actomyosin in transmitting such a signal. A single pulse of ATP localized in a 100-μm-wide stream was followed by a 300-μm-wide BBS stream (100 μM) to completely cover the area stimulated by the initial ATP stream. We followed the BBS stream with a second ATP stream at the same initial location to show that BBS treatment completely inhibited contraction both within the area stimulated by ATP as well as more distant tissue that responded to the initial stream of ATP (Fig. S4). Next, we wanted to assess the role of contractility in transmitting a signal rather than its role in effecting contraction. We applied a single pulse of ATP stimulation with a localized 100-μm-wide stream (Fig. 3*A*) followed by exposure to a stream of BBS that was narrower than the breadth of the contraction response (Fig. 3*B*). After a 2-h exposure to BBS we applied a second pulse of ATP in the same location as the original 100-μm stream of ATP (Fig. 3*C*) and found that BBS almost completely abolished ATP-induced contraction both within the region exposed to BBS as well as outside the BBS stream where the initial ATP stream had produced a contraction (Fig. 3 *D* and *E*). Within the region of ATP stimulation the BBS treatment reduced contraction, reducing the maximal strain from −0.09 to −0.002; in the region immediately outside the BBS domain contractions decreased from −0.05 to −0.002 (Fig. 3*F*). Furthermore, BBS reduced the distance of contractile signal transmission from 182 to 26 μm (Fig. 3*G*). Additionally, we used a similar approach to investigate the effect of BBS on the temporal and spatial limits of the contraction response and transmission (Fig. S5). Neither the magnitude of contraction nor the signal transmission distance of ATP-induced contraction changed in control experiments where explants were

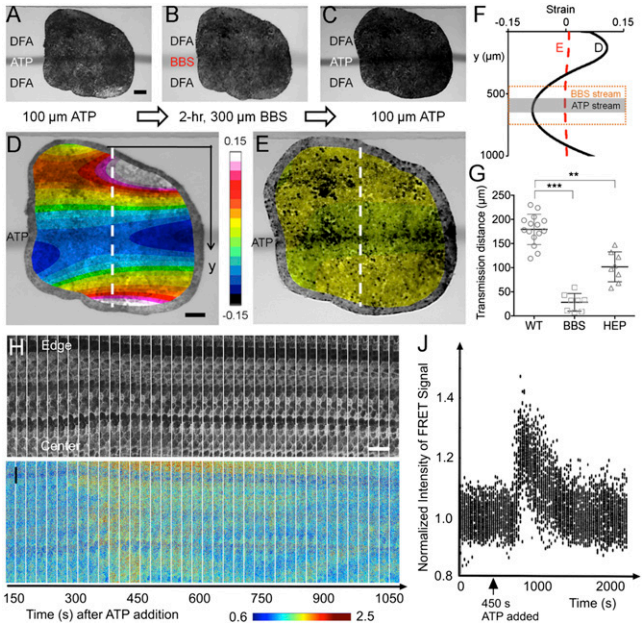

Fig. 3. Mechanochemical contractile signals through mechanical versus chemical cues. (*A*) Localized contraction was first triggered with a 100-μm ATP stream for 20 s at $t = 0$ s. (Scale bar: 100 μm.) (*B*) To disrupt actomyosin mechanical connections, this localized stimulation was followed by a 2-h BBS; actomyosin inhibitor) exposure to a 300-μm-wide lane that covers the location that the 100-μm ATP stream had previously stimulated (Fig. S4). (*C*) The same 100-μm ATP stream was applied for 20 s at $t = 2$ h immediately after the BBS was removed. (*D*) Image of a tissue overlaid with the strain map for the maximum contraction (at 40 s after the stimulation ends) of the tissue before being treated with BBS during ATP stimulation. (Scale bar: 100 μm.) (*E*) Image of the tissue overlaid with the strain map after being treated with BBS and then the ATP applied. (*F*) Effect of actomyosin inhibition on strain distribution in a tissue locally exposed to extracellular ATP. The black solid line is the initial strain distribution in the tissue from *D* when stimulated with 100-μm stream of extracellular ATP (indicated in dark gray). The red dashed line is the strain distribution in the tissue from *E* when stimulated with 100-μm stream of extracellular ATP after being exposed to BBS for 2 h, indicating almost no contraction after the addition of BBS that inhibits actomyosin activity. (*G*) Effects of actomyosin activity and gap junction on contractile signal transmission distance using BBS and HEP (gap-junction uncoupler). (For the detailed HEP experiments, see *Materials and Methods* and Figs. S7 and S8.) Error bars represent SDs (** indicates $P < 0.01$, *** indicates $P < 0.001$). (*H*) Maximal projection images from time-lapse confocal stacks in the donor emission channel show the morphology of the epithelial cells near their apical face and the expression of the biosensor. (Scale bar: 50 μm.) (*I*) Intensity of the FRET signal (Emission Acceptor–Emission of Donor) in the same sequence reveals that the Ca^{2+} response begins ~175 s after the start of the sequence, or 275 s after addition of ATP to the chamber, and sweeps from the exposed edge of the explant toward the center of the explant. (*J*) Normalized intensities of the FRET signals tracked within individual cells over time show that the spike and subsequent decay of calcium activity last ~10 min. Values in the graph represent average signal intensity of subdomains within the images normalized to the average intensity of the images before ATP addition. This result shows that tissue contraction corresponds to an influx of calcium within the responding tissues.

exposed to DMSO carrier for 2 h (Fig. S5*G*). Also, extended BBS treatment of half of the tissue did not alter local contraction response in the other half (Fig. S6), demonstrating that BBS effects are limited to exposed regions with no in-tissue diffusion. We do recognize the possibility that BBS-sensitive actomyosin contractility might be required for maintaining or establishing conventional signal transduction systems. Taken together, these findings indicate that signal transmission depends strongly on actomyosin contractility.

To test the role of gap junctions in transmitting the contraction signal, we used the gap-junction inhibitor heptanol (HEP) (25). We confirmed the effectiveness of this inhibitor by testing transmission of the small molecule lucifer yellow in *Xenopus* blastomeres (Fig. S7) (26). Due to the long incubation time needed to inhibit gap-junction function we treated whole embryos with 50 nM HEP from late blastula stages (stage 8) and cultured microsurgically isolated tissues in the HEP solution until the tissue spread within the microfluidic channel (approximately 5 h). After a 5-h exposure to the inhibitor (HEP), we applied a 20-s pulse of ATP (Fig. S8). The distance of contractile signal transmission was ~101 μm, which was 45% smaller than the control distance of 182 μm (Fig. 3*G*). In addition, we examined calcium signal propagation across the animal cap (AC). We collected confocal time-lapse imaging of stimulation with ATP and tracked the calcium response to show that tissue contraction coincides with an influx of calcium within the responding tissues (Fig. 3 *H*–*J*). Comparing strain distributions in globally disrupted gap-junction signaling and spatially disrupted nonmuscle myosin II, our findings indicate that contractility at a distance is greater after addition of HEP, which inhibits gap-junction signaling, than after treatment with BBS, which inhibits myosin II. In addition, both treatments significantly reduce the signal transmission distance compared with the control distance, indicating the transmission of signals triggered by ATP pass through adjacent tissues mediated via mechanical and chemical processes.

Considering the dynamic responses of the tissue contractility to periodic stimulations (Fig. S9; for analysis on dynamics and modeling see *SI Materials and Methods*), we sought to create an oscillating pattern of contraction within an epithelial sheet by treating the tissue as an actuator—a mechanical or biological mechanism that responds to a signal by converting an energy source into a force for creating movement; in our experiments, the signal is the application of ATP. The actuator is the collective cytoskeletal machinery of the cells of the AC tissue. To exert this level of control we empirically assessed the contractility response of tissues to periodic ATP stimulations (Fig. S9). We created a spatiotemporally periodic ATP profile to produce an oscillating contraction. To create an oscillation we initially positioned a

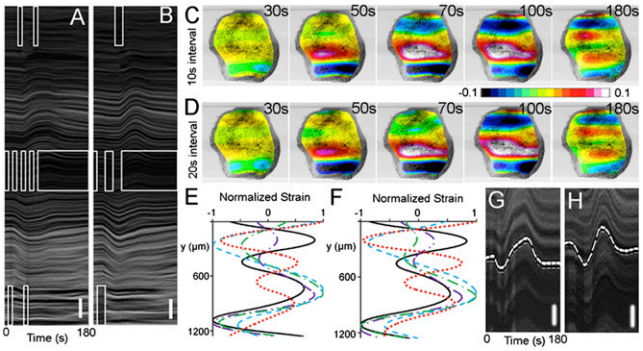

Fig. 4. Multisite coordinated tissue actuation propagates a wave-like contraction. (*A* and *B*) Kymographs show spatially and temporally varied cell movements in response to spatially varying ATP streams in square wave forms of (*A*) 10- and (*B*) 20-s intervals. The square waves have the 50% duty cycle with the periods of 20 s (10-s intervals) and 40 s (20-s intervals). [For the wave motion in the tissue see Movie S6 (10-s intervals) and Movie S7 (20-s intervals).] (Vertical scale bar: 100 μm.) The rectangular empty white boxes represent the positions of the ATP streams versus time. (*C* and *D*) Strain maps of the tissue at 30, 50, 70, 100, and 180 s after the periodic square wave stimulation at (*C*) 10- and (*D*) 20-s intervals. The contour colors represent strain from the initial tissue morphology. (*E* and *F*) Normalized strain distributions showing wave-like contractions after (*E*) 10- and (*F*) 20-s interval periodic stimulation after 30 s (black solid), 50 s (purple dot-dot-dash), 70 s (green dash-dot), 100 s (blue dash), and 180 s (red dot). (*G* and *H*) Marked wave patterns in kymographs perpendicular to the stream; (*G*) 10- and (*H*) 20-s intervals. The 20-s case exhibited a smooth wave form (e.g., sinusoidal wave) with a period of ~120 s. (Vertical scale bars: 50 μm.)

200-μm-wide stream of ATP at the vertical center region of the explant (Fig. S10*A*), moved it to the bottom edge after 10 or 20 s (Fig. S10*B*), and then moved the stream to the top edge after 10 or 20 s (Fig. S10*C*). This sequence produced two square waves in the position of the ATP stream with 10-s (Movie S6) or 20-s (Movie S7) dwell times at each location. The two driver profiles actuated contraction in two spatially and temporally distinct patterns observable in both kymographs (Fig. 4 *A* and *B*) and strain maps (Fig. 4 *C* and *D*). The oscillating strain produced "wave-like" phenomena over the tissue (Fig. 4 *E* and *F*; for side-by-side comparison see Fig. S11) and resulted in distinct wave patterns at the midline of the tissue (Fig. 4 *G* and *H* and Fig. S12). These findings imply that the sources of the differences between two intervals over the short term (10–30 s) result from signal transduction and cell contraction whereas viscous dissipation is a dominant driver over the longer term responses (more than 60 s; i.e., over the viscoelastic relaxation period). For example, the two short pulses and the single longer pulse produce slightly different strains in the tissue because the mechanical response to a single pulse is dissipated less than two shorter duration pulses. This is observed in the kymographs (Fig. 4 *A* and *B*) over the upper and lower domains of the tissue, as well as in the contractility responses of tissues to periodic ATP stimulations with different frequencies (Fig. S9).

Periodic ATP stimulation produces a wave-like contraction only if we stimulate the tissues multiple times at intervals that do not allow the tissue to fully relax. The wave-like nature of ATP-induced signals transmitted through tissues is investigated by directly measuring the wave velocity after ATP stimulation (Fig. S13). To characterize the wave-like response, we focused on a step input stimulation followed by a time analysis of the response of the contraction with respect to distance. Thus, the velocity of the wave could be obtained with respect to the contraction occurring over a distance. To accomplish this, a single short-duration pulse of a narrow stream of ATP was delivered to a local region of the tissue explants. We captured images of the response and applied an image analysis tool that uses registration algorithms from the open-source libraries of the Insight Toolkit to track displacement of small tissue patches (*Materials and Methods*). We tracked the area of these patches over the course of stimulation, contraction, and relaxation. This algorithm allowed a Lagrangian strain analysis of the deformation in the tissue frame of reference over time rather than an Eulerian analysis where strain was tracked in the laboratory frame of reference. This approach allowed us to estimate a wave velocity of ∼5 μm/s (Fig. S13). Such a wave velocity is sustained in *Xenopus* embryonic tissues rather than being immediately damped because the time constant of viscoelastic dissipation, ∼60 s, is longer than the time taken by a wave to pass through the tissue (18, 19). The kinematics of these wave-like contraction responses to periodic stimulations can be understood and predictably simulated using system dynamics theory. Signals that control cell behaviors or cell identities in tissues are generally transmitted via diffusion of bioactive compounds as in the case of morphogens (27) or propagated via electrical events such as action potentials in neuronal networks. The spreading of these activation waves depends on the principles of reaction diffusion and electrophysiology, respectively. In our case we propose a third mechanism observed in the *Xenopus* embryonic epithelium could be propagated by physical mechanical events. Because it takes ∼20 s for extracellular ATP to stimulate contractility, we rule out a "bucket-brigade" form of transmission (27) where one cell would release ATP upon stimulation, which would be sensed by an adjacent cell. Instead we propose that cells detect when their surfaces are mechanically stressed and then initiate a contractile response. We suspect cells detect stress rather than stretch or strain because we do not observe transient stretch as contractions spread from cells exposed to ATP (Fig. S13); however, it is possible that stretch is detected on the molecular or subcellular scales.

Conclusions

These coordinated responses indicate that tissue movements can be controlled in a manner that integrates both reception and transmission of activating signals and complex mechanical–contractile responses of individual cells within multicellular tissues and can be used to artificially create wave-like motions of contraction. Wave propagation is important in many physiological systems such as contraction of both adult and embryonic hearts (28) and may play a role in the control of epithelial contraction during embryonic morphogenesis (29, 30). Endogenous spontaneous Ca^{2+} waves within developing embryos have been observed for many years; for instance, waves have been observed during gastrulation and neurulation in *Xenopus laevis* and are generally thought to play a role in coordinating morphogenesis (31, 32). Also, traveling waves of contraction, often with Ca^{2+} waves, have been observed in many other systems including the coordination of cardiomyocyte contractility. Understanding the systems-level behavior of biological signaling networks may allow us to control biological actuators with engineered spatiotemporal stimulation. We believe our findings will provide a better understanding of contractility-dependent morphogenetic movements as well as the intercellular communication pathways critical during developmental biology, synthetic morphogenesis, and multicellular mechanotransduction signaling.

Materials and Methods

Embryo Handling and Microsurgery. Eggs from female *X. laevis* frogs were collected and fertilized in vitro through standard methods (33). The layers surrounding fertilized embryos were chemically removed by using 2% cysteine solution (pH 8) 1 h after fertilization. Embryos at the two-cell stage were cultured in 3% Ficoll (Sigma-Aldrich) in 1× MBS (modified Barth's solution). Embryos were cultured in 1/3× MBS to early gastrula stages (34). Vitelline membranes were manually removed using forceps before AC explants were microsurgically excised from stage 10 embryos with custom-made hair loops and hair knives in Danilchik's For Amy solution (DFA) (35) with BSA (0.2% in media; Sigma-Aldrich) and antibiotic–antimycotic (0.8% in media; A5955, Sigma-Aldrich). All of the compounds were stored and used according to the product guidelines (Sigma-Aldrich).

Strain Maps. Because deforming tissues can contain both actively contracting tissues and cells moving passively, the resulting displacements reflect both active responses by individual cells and passive responses by mechanically coupled cells. To help distinguish cells that actively contract from those that are displaced, we calculated the mechanical strain within the entire epithelium by comparing the sheet before stimulation to the maximally contracted sheet (strain in the direction perpendicular to the flow; ε_{yy}). We define the mechanical strain and calculate it in terms of local pixel-by-pixel deformation of the epithelium relative to its prestimulation shape (engineering strain defined as $\varepsilon = [[\text{length}_{\text{final}} - \text{length}_{\text{initial}}]/\text{length}_{\text{initial}}]$). Briefly, we collect images with a stereoscope at timed intervals. The light and dark regions in the images correspond to patterns of naturally occurring pigment in the apical surface of the cells. The time interval between images, typically a few seconds to minutes, is too short for significant cell rearrangement. Thus, tissue movements between these short intervals reflect contiguous deformation in the cell sheet. To calculate deformation we apply differential image correlation techniques (36) using custom image processing programs [from the NIH ImageJ plug-in bUnwarpJ (37)]. Because this method uses beta-splines the resulting deformations are "smooth." The units of deformation or displacement are pixels or micrometers per time interval and can be presented in either images (deformation maps; with intensity scaled to the real value of the *x*- or *y* displacement) or as arrays of arrows. We calculate the plane strains ε_{xx}, ε_{yy}, ε_{xy} by taking spatial gradients of the deformation vectors. Like deformation maps the strains fields can also be viewed as image maps with units of pixel–pixel per time-interval. Deformation and strain maps are displayed with false-color schemes (e.g., red–blue). Because the *y* axis corresponds to the axis transverse to the flow we typically use the ε_{yy} map in the figures to represent strain. Strain along a single path in the explant can be illustrated with a profile of ε_{yy} along a line in the image. Because strain measurements are collected over time intervals, strain maps and strain profiles represent strain rates, e.g., pixel–pixel per time interval. We assume actively contracting tissues exhibit negative strain, and cells moving passively are either stretched, indicated by positive strain, or simply displaced (i.e.,

moved without deformation), indicated by zero strain. Strains calculated in this way can be mapped over a bright-field image of the target tissue to produce a strain map that allows us to estimate how far a signal propagates from the site of direct stimulation. Time-lapse sequences collected from stereo microscope provide a set of information on the movements of tissues that are tracked. When analyzing localized ATP effects, there may be challenges with calculating the exact signal transmission distance. The transmission distance was ~50 μm greater when the tissues were exposed to the 100-μm-wide ATP stream than when exposed to the 500-μm-wide stream (Fig. 2 *B* and *D*). This significant difference in the signal transmission distance may result from the tissue boundary effect, which may lead to an imbalance of two mechanical forces between active contraction and passive tension in the cells that were not only receiving contractile signals but were also being mechanically stretched by neighboring contracted cells.

Assessing Gap-Junction Communication. To assess gap-junction communication in *Xenopus* embryonic cells, 1 cell out of an 8- or 16-cell embryo was injected with a 2:1 mixture of lucifer yellow (LY, 522 Da, Invitrogen) and rhodamine dextran (RD, 10 kDa, Invitrogen). LY moves across cells through gap junctions whereas RD does not due to their differential molecular size (26). Neighboring cells were monitored to determine which ones would have LY and RD versus cells with only LY. Gap-junction communication was interpreted to be the percentage of embryos that exhibited selective transfer of LY to neighboring cells during a 10-min period. The transfer of LY or RD was not detectable in the cells that were pretreated with HEP (0.5 mM, 1:1E5 diluted with DFA; Sigma-Aldrich) for 2 h; HEP uncouples gap junctions between cells (25, 38), In contrast, cells without HEP exhibited selective LY movement through gap junctions with no detectable transfer of RD in the tissue (Fig. S7).

Estimation of a Wave Velocity. The wave-like nature of ATP-induced signals transmitted through tissues was addressed by directly measuring the wave velocity after ATP stimulation. We focused on single short-duration pulses of a narrow stream of ATP delivered to tissue explants (Fig. S13). We applied a custom developed image analysis tool that uses registration algorithms from the open-source libraries of the Insight Toolkit (39) to track displacement of small tissue patches (~45 × 45-μm square) containing ~5–10 cells. To estimate the velocity of the contraction wave we focused on the contractile response when the acceleration of the contraction reversed sign. This inflection time point was found when the area of a patch [fit with a spline function, $f(t)$] reached its maximum rate of contraction [e.g., $f''(t) = 0$]. The inflection time occurred before the time of maximum contraction and would be less affected by secondary time-dependent processes. Thus, the inflection point is a conservative estimate of the rate of wave propagation in this tissue. From this analysis we estimated the wave propagation was ~5 μm/s.

ACKNOWLEDGMENTS. We thank Yingxiao Peter Wang for kindly providing the plasmid encoding the calcium FRET biosensor and John Wallingford and Richard Harland for the plasmids encoding the membrane-targeted GFP. This work was supported in part by the National Science Foundation (CMS0555513, CAREER IOS-0845775, and CMMI-1100515), the Office of Naval Research, the National Institutes of Health (R01-HD044750 and R21 ES019259), the Air Force Office of Scientific Research (FA9550-13-1-01 08), the National Science Foundation (CMMI-1100430, CMMI-1160840, CPS-1135850), the Sloan Foundation, Biomechanics in Regenerative Medicine T32-EB003392 (to D.S.V.), Cardiovascular Bioengineering Training Program T32-HL076124 (to T.R.J.), and the American Heart Association (Beginning Grant-in-Aid).

1. Gorfinkiel N, Blanchard GB (2011) Dynamics of actomyosin contractile activity during epithelial morphogenesis. *Curr Opin Cell Biol* 23(5):531–539.
2. Sawyer JM, et al. (2010) Apical constriction: A cell shape change that can drive morphogenesis. *Dev Biol* 341(1):5–19.
3. Martin AC, Gelbart M, Fernandez-Gonzalez R, Kaschube M, Wieschaus EF (2010) Integration of contractile forces during tissue invagination. *J Cell Biol* 188(5):735–749.
4. Tsuno A, et al. (2009) Decidualization attenuates the contractility of eutopic and ectopic endometrial stromal cells: Implications for hormone therapy of endometriosis. *J Clin Endocrinol Metab* 94(7):2516–2523.
5. Meziani F, et al. (2006) Shed membrane particles from preeclamptic women generate vascular wall inflammation and blunt vascular contractility. *Am J Pathol* 169(4):1473–1483.
6. Montell DJ (2008) Morphogenetic cell movements: Diversity from modular mechanical properties. *Science* 322(5907):1502–1505.
7. Chauhan BK, Lou M, Zheng Y, Lang RA (2011) Balanced Rac1 and RhoA activities regulate cell shape and drive invagination morphogenesis in epithelia. *Proc Natl Acad Sci USA* 108(45):18289–18294.
8. Poincloux R, et al. (2011) Contractility of the cell rear drives invasion of breast tumor cells in 3D Matrigel. *Proc Natl Acad Sci USA* 108(5):1943–1948.
9. Quintana L, et al. (2009) Early tissue patterning recreated by mouse embryonic fibroblasts in a three-dimensional environment. *Tissue Eng Part A* 15(1):45–54.
10. Kerszberg M, Wolpert L (2007) Specifying positional information in the embryo: Looking beyond morphogens. *Cell* 130(2):205–209.
11. Lawrence PA, Levine M (2006) Mosaic and regulative development: Two faces of one coin. *Curr Biol* 16(7):R236–239.
12. Follonier L, Schaub S, Meister JJ, Hinz B (2008) Myofibroblast communication is controlled by intercellular mechanical coupling. *J Cell Sci* 121(Pt 20):3305–3316.
13. Hinz B, Pittet P, Smith-Clerc J, Chaponnier C, Meister JJ (2004) Myofibroblast development is characterized by specific cell-cell adherens junctions. *Mol Biol Cell* 15(9):4310–4320.
14. Na S, et al. (2008) Rapid signal transduction in living cells is a unique feature of mechanotransduction. *Proc Natl Acad Sci USA* 105(18):6626–6631.
15. Weber GF, Bjerke MA, Desimone DW (2012) A mechanoresponsive cadherin-keratin complex directs polarized protrusive behavior and collective cell migration. *Dev Cell* 22(1):104–115.
16. Joshi SD, von Dassow M, Davidson LA (2010) Experimental control of excitable embryonic tissues: Three stimuli induce rapid epithelial contraction. *Exp Cell Res* 316(1):103–114.
17. Ralevic V, Burnstock G (1998) Receptors for purines and pyrimidines. *Pharmacol Rev* 50(3):413–492.
18. von Dassow M, Strother JA, Davidson LA (2010) Surprisingly simple mechanical behavior from a complex embryonic tissue. *PLoS ONE* 5(12):e15359.
19. Zhou J, Kim HY, Davidson LA (2009) Actomyosin stiffens the vertebrate embryo during critical stages of elongation and neural tube closure. *Development* 136(4):677–688.
20. Martin AC, Kaschube M, Wieschaus EF (2009) Pulsed contractions of an actin-myosin network drive apical constriction. *Nature* 457(7228):495–499.
21. David DJ, Tishkina A, Harris TJ (2010) The PAR complex regulates pulsed actomyosin contractions during amnioserosa apical constriction in Drosophila. *Development* 137(10):1645–1655.
22. Kim HY, Davidson LA (2011) Punctuated actin contractions during convergent extension and their permissive regulation by the non-canonical Wnt-signaling pathway. *J Cell Sci* 124(Pt 4):635–646.
23. Allingham JS, Smith R, Rayment I (2005) The structural basis of blebbistatin inhibition and specificity for myosin II. *Nat Struct Mol Biol* 12(4):378–379.
24. Straight AF, et al. (2003) Dissecting temporal and spatial control of cytokinesis with a myosin II Inhibitor. *Science* 299(5613):1743–1747.
25. Georgescu A, Alexandru N, Constantinescu E, Popov D (2006) Effect of gap junction uncoupler heptanol on resistance arteries reactivity in experimental models of diabetes, hyperlipemia and hyperlipemia-diabetes. *Vascul Pharmacol* 44(6):513–518.
26. Levin M, Mercola M (1998) Gap junctions are involved in the early generation of left-right asymmetry. *Dev Biol* 203(1):90–105.
27. Lander AD, Nie Q, Wan FY (2002) Do morphogen gradients arise by diffusion? *Dev Cell* 2(6):785–796.
28. Forouhar AS, et al. (2006) The embryonic vertebrate heart tube is a dynamic suction pump. *Science* 312(5774):751–753.
29. Solon J, Kaya-Copur A, Colombelli J, Brunner D (2009) Pulsed forces timed by a ratchet-like mechanism drive directed tissue movement during dorsal closure. *Cell* 137(7):1331–1342.
30. Martin AC (2010) Pulsation and stabilization: Contractile forces that underlie morphogenesis. *Dev Biol* 341(1):114–125.
31. Wallingford JB, Ewald AJ, Harland RM, Fraser SE (2001) Calcium signaling during convergent extension in Xenopus. *Curr Biol* 11(9):652–661.
32. Shindo A, et al. (2010) Tissue-tissue interaction-triggered calcium elevation is required for cell polarization during Xenopus gastrulation. *PLoS ONE* 5(2):e8897.
33. Kay BK (1991) Xenopus laevis: Practical uses in cell and molecular biology. Injections of oocytes and embryos. *Methods Cell Biol* 36:663–669.
34. Nieuwkoop PD (1967) The "organization centre." 3. Segregation and pattern formation in morphogenetic fields. *Acta Biotheor* 17(4):178–194.
35. Sater AK, Steinhardt RA, Keller R (1993) Induction of neuronal differentiation by planar signals in *Xenopus* embryos. *Dev Dyn* 197(4):268–280.
36. Sutton MA, Orteu JJ, Schreier HW (2009) *Image Correlation for Shape, Motion and Deformation Measurements: Basic Concepts, Theory, and Applications* (Springer, New York).
37. Ooi MB, et al. (2013) Combined prospective and retrospective correction to reduce motion-induced image misalignment and geometric distortions in EPI. *Magn Reson Med* 69(3):803–811.
38. Li G, Whittaker P, Yao M, Kloner RA, Przyklenk K (2002) The gap junction uncoupler heptanol abrogates infarct size reduction with preconditioning in mouse hearts. *Cardiovasc Pathol* 11(3):158–165.
39. Yoo TS, et al. (2002) Engineering and algorithm design for an image processing API: A technical report on ITK-the Insight Toolkit. *Stud Health Technol Inform* 85:586–592.
40. Kim Y, LeDuc P, Messner W (2013) Modeling and control of a nonlinear mechanism for high performance microfluidic systems. *IEEE Trans Contr Syst Technol* 21(1):203–211.
41. Kim Y, Joshi SD, Messner WC, LeDuc PR, Davidson LA (2011) Detection of dynamic spatiotemporal response to periodic chemical stimulation in a Xenopus embryonic tissue. *PLoS ONE* 6(1):e14624.
42. Kim Y, Kuczenski B, LeDuc PR, Messner WC (2009) Modulation of fluidic resistance and capacitance for long-term, high-speed feedback control of a microfluidic interface. *Lab on a chip* 9(17):2603–2609.